Journal of Magnetism and Magnetic Materials 324 (2012) 2011–2018

Contents lists available at SciVerse ScienceDirect

Journal of Magnetism and Magnetic Materials

journal homepage: www.elsevier.com/locate/jmmm

Magnetic, structural, and transport properties at very high temperature in manganites

Fabian Enrique Nima Ramirez, Fabio Furlan Ferreira, Wendel Andrade Alves, José Fernando Queiruga Rey, José Antonio Souza *

Centro de Ciências Naturais e Humanas, Universidade Federal do ABC, Santo André, CEP 09090-400, SP, Brazil

ARTICLE INFO

Article history:
Received 21 December 2011
Available online 10 February 2012

Keywords:
Manganite
Phase transition
Polaron mechanism
Spin-lattice-charge coupling

ABSTRACT

Magnetic, structural, and electric transport measurements at high temperatures were carried out on $La_{1-x}Ca_xMnO_3$; $x=0.20$, 0.25, 0.30, 0.34, 0.40, and 0.45. All samples show a first-order structural phase transition from orthorhombic *Pnma* to rhombohedral $R\bar{3}c$ space group at T_{R-O}. Magnetic susceptibility measurements show that the Curie–Weiss law is strictly obeyed in the rhombohedral phase as opposed to the orthorhombic phase where the effective magnetic moment has a temperature dependence. The electrical resistivity is well described by the small polaron hopping mechanism in the samples up to $x=0.34$. As the charge carriers are introduced into the system ($x=0.40$ and 0.45), this mechanism of hopping ceases to be valid. The value of Grüneisen parameter obtained through analysis of high-resolution X-ray powder diffraction as a function of temperature increases abruptly for the sample with $x=0.40$. This is consistent with an increase in bending and stretchinglike frequency modes observed by Raman spectroscopy.

1. Introduction

The microscopic mechanism underlying electronic, structural, and magnetic properties in strong spin–lattice–charge coupled systems is a subject of great interest in condensed matter physics [1]. The prototypal spin–charge–lattice coupled manganese perovskite $LaMnO_3$ is an antiferromagnetic and insulating system [2,3]. The introduction of holes (Mn^{4+}) into the Mn^{3+} e_g orbitals creates ferromagnetic double exchange interactions which couples the magnetic system with electrical conductivity [4], while Jahn–Teller distorted ions Mn^{3+} couple the magnetic and lattice degrees of freedom. This unusually strong coupling between the electronic, magnetic, and structural properties is suggested to bring about the colossal magnetoresistance effect [5,6]. Once the correlation among degrees of freedom is achieved a better understanding of the thermodynamic quantities of these systems will emerge. However, structural, magnetic, and electrical conductivity studies at very high temperatures in those systems are scarce in the literature. This has led to difficulties in understanding the order parameters and the coupled physical properties of the system.

In general, it is well accepted that the electrical transport mechanism of manganites is well described by the small polaron hopping [7–9]. The localized carriers distort the surrounding lattice exchanging energy and thus forming a bounded polaron. In a simplified approach for manganites, a small lattice polaron can be formed when an e_g electron localizes on a Mn^{3+} ion, and the surrounding oxygen octahedron is distorted due to the Jahn–Teller (JT) effect.

On the other hand, it is not known if there exists a limit at which this model ceases to be valid when charge carriers are varied. Several works have shown that this model fails for some manganite systems, but there is no systematic study revealing the driven physical parameter responsible for deviations from small polaron mechanism [9–14]. Nevertheless, in general those fittings are made at intermediate temperature, close to the ferromagnetic transition, where fluctuations of the clustered magneticlike environment surrounding small polarons influence strongly the electrical transport mechanism [11–14]. In addition, most of the literature is focused on the interplay between magnetic and transport properties, and no systematic study has been made to understand the correlations between the electrical resistivity and crystal structure in the paramagnetic semiconducting state.

In this work, we show that the small polaron hopping mechanism ceases to be valid as charge carriers are introduced into the system. The magnetic results indicate no significantly evidence of direct correlation between the breakdown of transport mechanism and the increase of the effective magnetic moment. Measurements of high-resolution X-ray power diffraction and Raman spectroscopy were put forward to obtain insight on nature of

* Corresponding author.
E-mail address: joseantonio.souza@ufabc.edu.br (J.A. Souza).

0304-8853
doi:10.1016/j.jmmm.2012.01.036

charge and lattice correlation. We have observed that such a deviation from small polaron hopping mechanism is consistent with an increase in the Grüneisen parameter. The electrical resistivity value at room temperature is suggested to be related to the abrupt change in the bending and stretching modes as charge carriers are introduced into the system.

2. Experimental

Polycrystalline samples of $La_{1-x}Ca_xMnO_3$ were prepared by sol–gel method. Samples prepared through this chemical route have better chemical homogeneity than when using the standard solid-state reaction method. Stoichiometric amounts of hydrated manganese acetate ($C_4H_6MnO_4 \cdot 4H_2O$) and nitrates of the remaining cations were dissolved in distilled water containing a 50 mol% excess of citric acid and ethylene glycol. The polymeric precursor was formed by heating and stirring the solution at 120 °C. After a few hours a gel is formed, and then dried. The organic material was oxidized 24 h at 600 °C. The powder was ground with an agate mortar for 30 min, heat treated 15 h at 1000 °C. This last step was repeated three times with reaction temperatures of 1050 °C, 1100 °C and 1300 °C. Finally, the powder was ground for 30 min, pressed into pellets and reacted 40 h at 1350 °C. The density of our samples is very high approximately 97% of theoretical density. The X-ray powder diffraction indicates that all samples are single phase belonging to orthorhombic space group *Pnma*. The average Mn oxidation state was determined by iodometric titration. The titration procedure was repeated at least three times for each sample. The titration experiment determines the average Mn valence under the assumption that the valences of La, Ca, and O are +3, +2, and −2. It is well known that these Mn oxides possess La and Mn defects rather than an oxygen excess. The obtained average Mn valence was 3.23(1), 3.27(1), 3.32(1), 3.35(1), 3.42(1), 3.46(1) for $x=0.20$, 0.25, 0.30, 0.34, 0.40, and 0.45, respectively. Magnetization measurements (from 10 K to 900 K) were performed using a standard vibrating sample magnetometer (VSM) oven option from Quantum Design. Electrical resistivity was measured using a four-probe method using a home-made apparatus with a platinum thermometer mounted close to the sample. Silver epoxy was used to make contacts to the sample. Data were collected in air on warming to the highest temperature followed by cooling. We have performed both thermogravimetric analysis (TGA) and differential scanning calorimetry (DSC) up to 950 K (not shown). DSC shows a robust peak indicating a phase transition for the samples and TGA revealed no changes in the studied temperature range, indicating negligible oxygen loss. High-resolution X-ray powder-diffraction (HRXPD) measurements were conducted on the XPD beamline at the Laboratório Nacional de Luz Síncrotron [15]. The sintered pellet was ground and sieved to reject grains larger than ~5 μm. Wavelength of 1.240 and 2θ steps of 0.005° were chosen for our measurements. A furnace with Ar flow was employed for the high-temperature measurements. Raman spectra were recorded in a Renishaw Raman System 3000 spectrometer, with a CCD detector, coupled to an Olympus BTH2 microscope (80-fold enhancement). A He–Ne laser (Spectra Physic, model 127) with excitation radiation at 632.8 nm, was used.

3. Results and discussion

In Fig. 1 the electrical resistivity as a function of temperature is presented for all samples studied herein, $x=0.20$, 0.25, 0.30, 0.34, 0.40, and 0.45. A thermally activated electrical transport mechanism—semiconductinglike behavior is clearly observed for

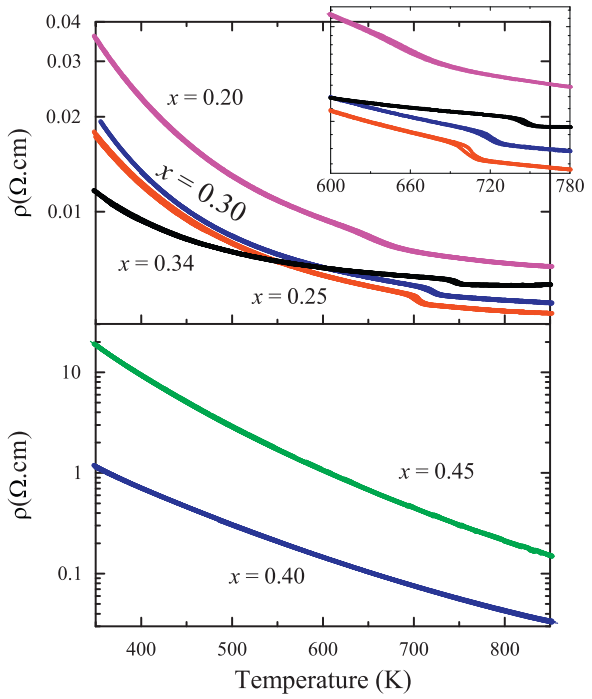

Fig. 1. Electrical resistivity as a function of temperature for $La_{1-x}Ca_xMnO_3$, $x=0.20$, 0.25, 0.30, 0.34, 0.40, and 0.45. The inset shows a thermal hysteresis in the samples with $x=0.20$, 0.25, 0.30, and 0.34 due to a structural phase transition from orthorhombic (O) to rhombohedral (R) space group.

all samples. It is known that this family $La_{1-x}Ca_xMnO_3$ shows an orthorhombic to rhombohedral structural phase transition T_{R-O} at high temperatures [16]. In samples with $x=0.20$, 0.25, 0.30, and 0.34, this structural phase transition brings about a hysteretic behavior at T_{R-O} revealing the first order nature of the transition. Interestingly, neither a hysteretic behavior nor any feature is detected in samples with $x=0.40$ and 0.45 by the electrical resistivity measurements. As we shall see in the unit-cell parameters obtained by high-resolution X-ray diffraction data the sample with $x=0.45$ also undergoes a structural phase transition, even though not visible by the electrical resistivity data. Furthermore, it is observed that as charge carriers are introduced into the system, the electrical resistivity decreases and abruptly increases above $x=0.40$. The value measured in the samples with $x=0.20$, 0.25, 0.30, and 0.34 is in the range of 0.01−0.04 Ω cm, while in the samples with $x=0.40$ and 0.45 it is in the range of 1−20 Ω cm. The magnitude of the electrical resistivity close to T_{R-O} in samples $x=0.20$, 0.25, 0.30 and 0.34 has the same order (5 mΩ cm) as that found in manganites with bad metal behavior [17], suggesting a more delocalized character of the charge carriers.

The electrical resistivity in the small polaron model may be expressed as [7,18]

$$\rho(T) = AT^s \exp(E_p/k_BT) \quad (1)$$

where A is a pre-factor, E_p is the polaron activation energy, and k_B is the Boltzmann constant. In the adiabatic regime $s=1$ (non-adiabatic regime $s=3/2$), the hopping of electrons is faster (slower) than the vibration of the optical phonon mode [7,8,19].

In Fig. 2, we plot the data assuming both adiabatic and nonadiabatic regimes for samples with $x=0.20$, 0.25, 0.30, and 0.34. As can be observed, all samples may be fitted using those regimes in both rhombohedral and orthorhombic phases. In a previous work, Souza et al. [19] showed that a temperature dependence of electrical resistivity in high temperatures for $x=0.30$ can be explained by the small polaron hopping mechanism. They observed a subtle change from adiabatic to nonadiabatic

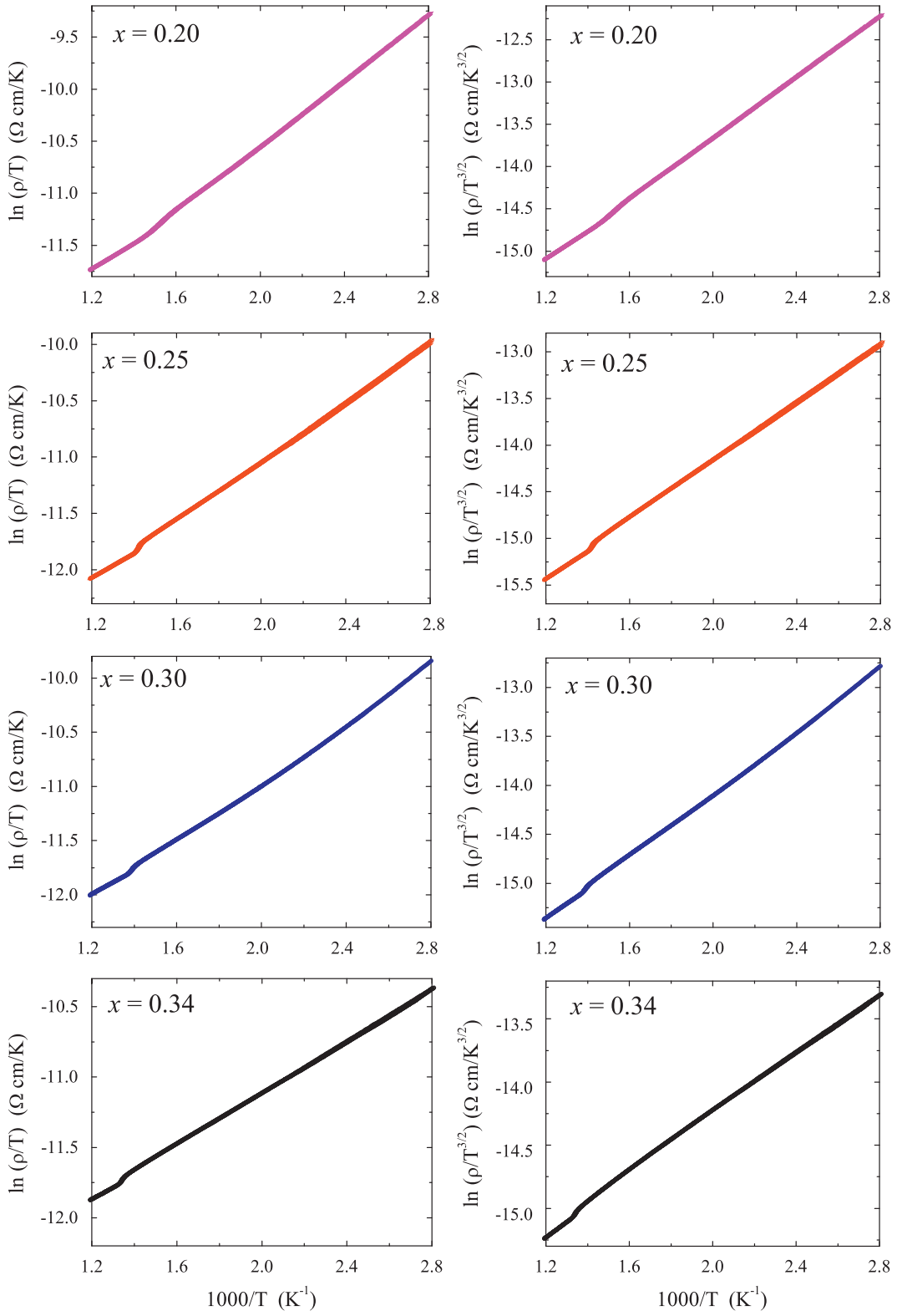

Fig. 2. The ρ (T) is plotted in the adiabatic ($s=1$) and nonadiabatic ($s=3/2$) small polaron hopping regimes for the samples with $x=0.20$, 0.25, 0.30, and 0.34.

regime, when the crystal structure changes from rhombohedral ($T > T_{R-O}$) to orthorhombic ($T < T_{R-O}$) crystalline system. However, the results displayed in Fig. 2 reveal that, overall, it is a difficult task to discriminate whether the regime is adiabatic or nonadiabatic in each crystallographic phase.

The values of the polaron activation energy calculated by fitting both nonadiabatic and adiabatic regimes are indicated in Table 1. It is observed that for the samples with $x=0.20$, 0.25, and 0.30, the values of the polaron activation energy decreases when the structure moves from *Pnma* to $R\bar{3}c$ phase, in both nonadiabatic and adiabatic regimes. However, for the sample with $x=0.34$, the value of the polaron activation energy increases slightly, when the structure moves from *Pnma* to $R\bar{3}c$ phase in the nonadiabatic regime. Since the electrical resistivity decreases,

it may not be physically acceptable. Probably in this sample, the structural phase transition is accompanied by a change from nonadiabatic to adiabatic regime as it is the case for the sample with $x=0.30$. Therefore, the abrupt decreasing in the electrical resistivity observed close to the T_{R-O} due to the structural phase transition is more likely to be associated with a decreasing in the polaron activation energy (E_p) for the samples with low charge carriers. On the other hand, the data suggest a change from nonadiabatic to adiabatic regime in the samples with $x=0.30$ and 0.34 as the system goes to rhombohedral phase.

In Fig. 3, the adiabatic and nonadiabatic regimes are evaluated for the high-resistivity samples, $x=0.40$ and 0.45. As the charge carriers are further introduced into the structure, the small polaron hopping mechanism fails to describe the electrical transport in this system. It is found a pronounced curvature instead of linearity over the entire studied temperature range in both samples indicating complete deviations from small polaron hopping model. Both Arrhenius and variable-range-hopping (VRH) models were also checked to describe the temperature dependence of the electrical resistivity. These models also do not fit the transport mechanism in these samples. It is important to emphasize that the studied temperature interval here is much higher than $\Theta_D/2$ (Θ_D stands for the Debye temperature). On the other hand, the high T interval is also required as long as fluctuation of magnetic short range order close to the ferromagnetic phase transition may strongly influence the electrical transport [20]. Therefore, we suggest that the electrical resistivity in these samples deserves further attention in order to understand how charge carriers involve themselves as temperature and crystal structure are changed. To accomplish this task, we have measured magnetic susceptibility and high resolution X-ray powder diffraction in the same temperature interval for two samples: one that the transport mechanism is described by the small polaron hopping; and another one that this mechanism fails.

Table 1
Values of the E_p calculated from fitting the nonadiabatic and adiabatic regimes for the samples with $x=0.20$, 0.25, 0.30, and 0.34.

Sample	Nonadiabatic		Adiabatic	
	E_p[a] (meV)	E_p[b] (meV)	E_p[a] (meV)	E_p[b] (meV)
$x=0.20$	155.4(4)	137.5(3)	135.4(1)	103.9(5)
$x=0.25$	133.1(2)	125.8(3)	112.0(8)	91.2(7)
$x=0.30$	132.7(1)	127.5(1)	110.4(2)	92.9(3)
$x=0.34$	100.2(1)	103.1(2)	78.6(3)	67.8(2)

[a] *Pnma*.
[b] $R\bar{3}c$.

In Fig. 4, we show the inverse of χ as a function of the temperature for $x=0.25$ and 0.45 which reveals clearly the structural phase transition at T_{R-O}. The T-independent atomic core diamagnetic and Van Vlack susceptibility contributions were subtracted [21]. The values of the T_{R-O} obtained for all samples (not shown) through magnetic data are in agreement with the phase diagram [16]. A linear behavior of χ^{-1} vs. T is observed *only* above T_{R-O} indicating that the Curie–Weiss law is obeyed, suggesting that the Mn^{4+} and Mn^{3+} ions are totally free in the rhombohedral phase.

The expected value of the effective magnetic moment, assuming orbital quenching, is $p_{eff}=g\sqrt{xS_1(S_1+1)+(1-x)S_2(S_2+1)}$, where $g=2$, $S_1=3/2$ and $S_2=2$ for Mn^{4+} and Mn^{3+}, respectively [22]. Furthermore, the slope (A) of χ^{-1} vs. T is proportional to the effective magnetic moment. Thus, $p_{eff}\,(\mu_B)=2.82\sqrt{1/A}$ when χ^{-1}(mole Oe/emu). We estimate the effective magnetic moment in $T>T_{O-R}$ and the obtained values are in very good agreement with expected for spin-only ions Mn^{4+}/Mn^{3+} in the rhombohedral phase. On the other hand, below T_{R-O} a large curvature in χ^{-1} vs. T is observed indicating deviation from Curie–Weiss law. The nonlinear behavior of $\chi\,(T)$ can be confirmed by the derivative $d\chi/dT$ shown in the insets of the Fig. 3.

In order to carefully compare the magnetic evolution of samples with different transport mechanisms, we have estimated the effective magnetic moment of the selected samples by taking into account the slope of a linear fit in every 10 K interval. Fig. 5 shows the effective magnetic moment of the samples with

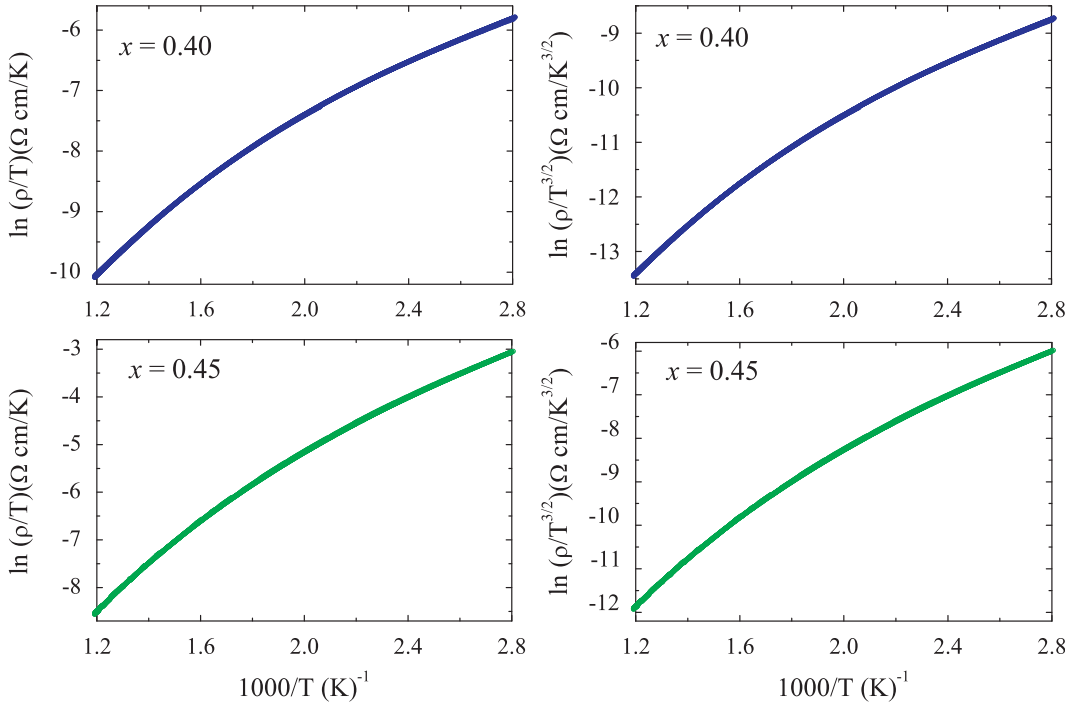

Fig. 3. The $\rho\,(T)$ is plotted in the adiabatic ($s=1$) and nonadiabatic ($s=3/2$) small polaron hopping regimes for the samples with $x=0.40$ and 0.45.

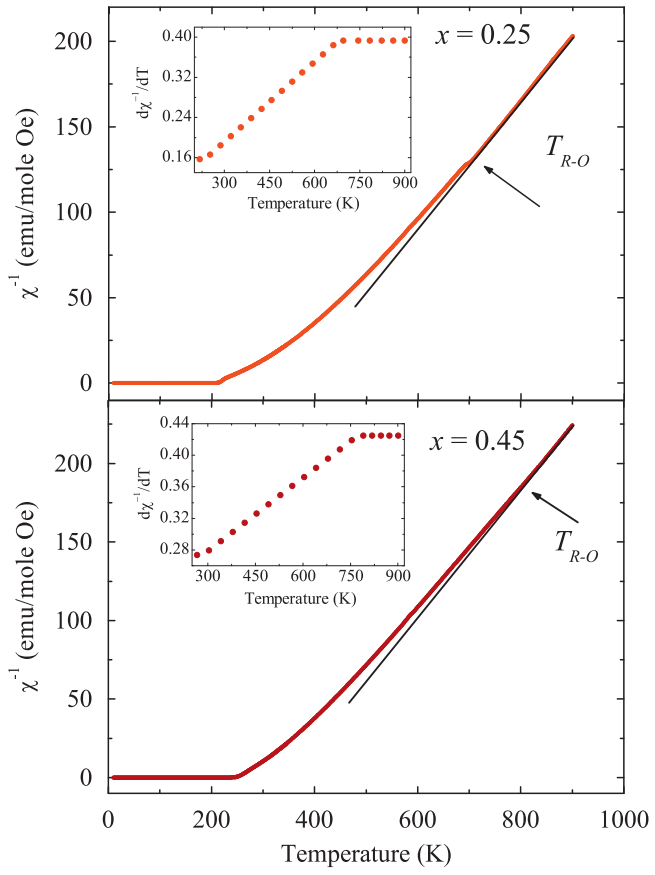

Fig. 4. Temperature dependence of the inverse of magnetic susceptibility as a function of temperature for the samples with $x=0.25$ and 0.45. The inset indicates the nonlinear and linear behavior below and above of the T_{R-O}, respectively.

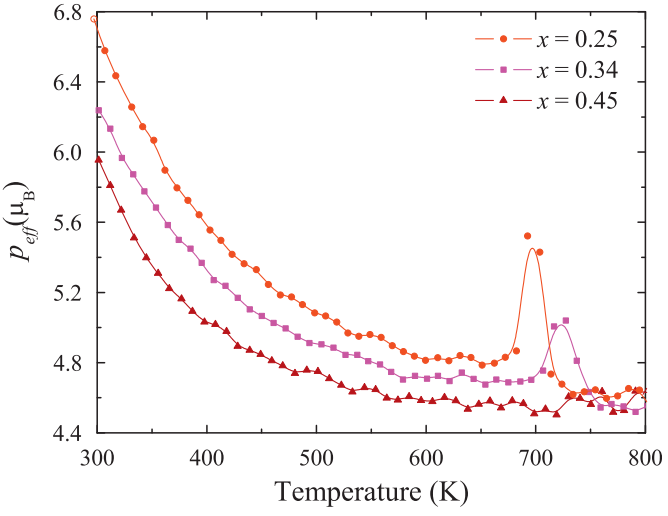

Fig. 5. The effective magnetic moment as a function of the temperature for selected samples.

$x=0.25$, 0.34, and 0.45 as function of the temperature. It is observed that (i) the effective magnetic moment decreases with increasing Mn^{4+} concentration and more importantly (ii) the temperature dependence of the p_{eff} is charge carrier independent. Indeed, the curve p_{eff} vs. T for different values of x exhibits the same behavior. Interestingly, while the transport mechanism changes with the increasing of number of charge carriers, the temperature dependence of the effective magnetic moment is not significantly influenced by these changes in the orthorhombic phase. These results suggest that the magnetic properties are not directly correlated to the change in the transport mechanism.

We have done Rietveld refinements of the high resolution X-ray powder diffraction data for $La_{0.70}Ca_{0.30}MnO_3$ and $La_{0.55}Ca_{0.45}MnO_3$ (not shown). Fig. 6 shows the temperature dependence of the unit-cell parameters a, $b/\sqrt{2}$, c, and unit-cell volume (V) of both samples. A monoclinic unit-cell setting was adopted for the rhombohedral phase allowing a direct comparison with the orthorhombic lattice parameters [24].

In the sample with $x=0.30$, an orthorhombic structure with space group *Pnma* is observed up to $T_{R-O}\sim 690$ K, while a rhombohedral structure with space group $R\bar{3}c$ is observed above $T_{R-O}\sim 720$ K. In between, both phases coexist. This structural phase transition was also detected in both electrical resistivity and magnetic susceptibility results. The sample with $x=0.45$ exhibits a partial structural phase transition at $T_{R-O}\sim 767$ K, above this temperature ($767\ \text{K} < T < 891\ \text{K}$) both phases coexist in the whole studied temperature range. At 891 K, we still observed a volume fraction of 10% of orthorhombic *Pnma* space group (90% rhombohedral $R\bar{3}c$). This structural transition was not detected by the electrical resistivity measurements. The absence of thermal hysteresis in the electrical resistivity may be likely associated with the partial structural phase transition nature.

We believe that the difference found in the electronic transport mechanism between both samples as charge carriers are introduced is closely related to the thermal expansion coefficient. Thus, we fit the unit-cell volume of the two samples using a second order polynomial, as shown in Fig. 7. The results indicate that for the sample with $x=0.45$, the volumetric thermal expansion coefficient is temperature independent whereas in the sample with $x=0.30$ shows a linear temperature dependence.

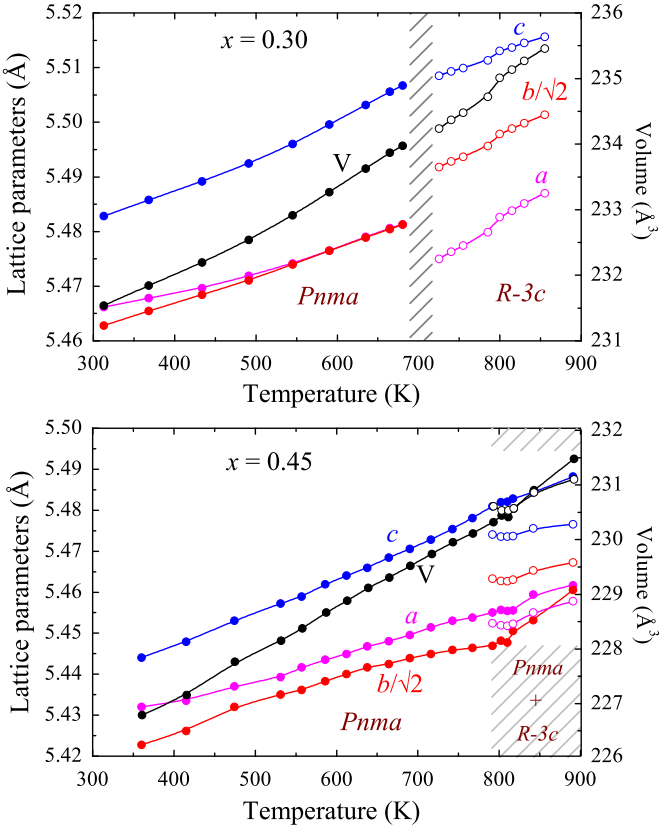

Fig. 6. Temperature dependence of lattice parameters and unit-cell volume for $x=0.30$ (upper panel) and $x=0.45$ (lower panel). Solid symbols and open symbols represent parameters for *Pnma* phase and $R\bar{3}c$ phase, respectively. Shaded area indicates the coexistence of orthorhombic and rhombohedral phases.

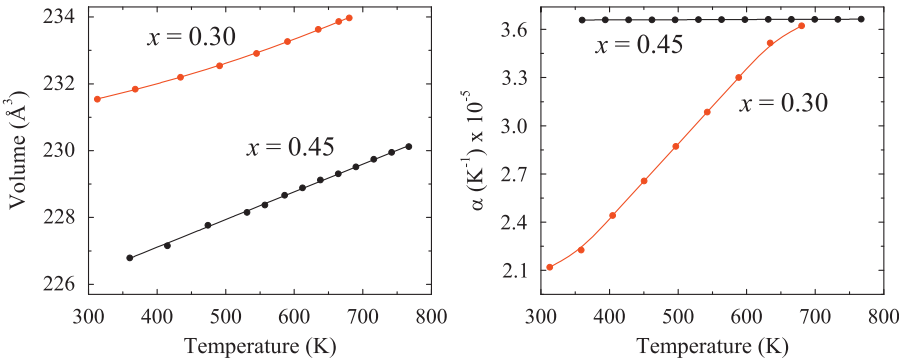

Fig. 7. Left panel shows the unit-cell volume as a function of the temperature for the sample with $x=0.30$ and 0.45. Solid lines represent the fit with a second order polynomial. Right panel shows the volumetric thermal expansion coefficient as a function of the temperature for the sample with $x=0.30$ and 0.45.

As discussed above, the electrical resistivity of the sample $x=0.30$ is much smaller than in the sample $x=0.45$. The electrical resistivity of this sample close to T_{R-O}, was found to be consistent with that of bad metals. The more delocalized character of the charge carriers in the sample with $x=0.30$ increases significantly the electronic contribution to the internal energy of the system, as suggested by the results shown in the Fig. 7. Overall, the dc/dT is $\sim$1.4 times higher than da/dT and db/dT for the sample with $x=0.30$ and $\sim$2.5 times higher than da/dT and db/dT for the sample with $x=0.45$. Therefore, the parameter c has more influence on the thermal expansion of the unit cell on both samples. For the phase $R\bar{3}c$, we have observed a more isotropic character of the unit-cell thermal expansion. A carefully inspection of Fig. 6 shows that the crystal strain $s=(a-b)/2(a+b)$ due to orthorhombic distortion remains roughly constant for the sample with $x=0.45$ whereas it decreases quickly and goes to zero for the sample with $x=0.30$.

In order to further understand the thermal expansion behavior which may be coupled to the electronic transport mechanism, we have fitted the data using the anharmonic theory [23]. In this theory, the volume and the thermal expansion coefficient, taking into account only the anharmonic vibrations of atoms and using the Debye model for the lattice internal energy, are given, respectively, by [25,26]

$$V(T)\cong V(T=0)+\frac{9\gamma Nk_B}{B}(T)^1\left(\frac{T}{\Theta_D}\right)^3\int_0^{\Theta_D/T}\frac{x^3}{e^x-1}\,dx \tag{2}$$

$$\frac{dV}{dT}\cong\frac{9\gamma Nk_B}{B}(T)^0\left(\frac{T}{\Theta_D}\right)^3\int_0^{\Theta_D/T}\frac{e^x x^4}{e^x-1}\,dx \tag{3}$$

where $V(T=0)$, Θ_D, B, and γ stand for the volume at 0 K, the Debye temperature, the bulk modulus, and the Grüneisen parameter, respectively. This latter parameter is related to the variation, with respect to volume, of the frequency of the phonon mode $[\mathrm{d}(\ln \nu)/\mathrm{d}(\ln V)]=-\gamma$. In order to accomplish this task, we let $V(T=0)$, Θ_D, and $9\gamma Nk_B/B$ be free fitting parameters. The temperature dependence of the volume along with the fitting using Eq. (2) is shown in Fig. 8. At high temperatures, Eq. (2) has an almost linear behavior with respect to temperature and Eq. (3) shows a temperature independent behavior [23]. This prediction is in line with the behavior observed for $x=0.45$ sample, see Fig. 7. This result suggests that the phonon contribution is dominant for this sample and more in line with Debye lattice model.

The obtained parameters from the fitting are shown in Table 2. It is observed an increase in the Debye temperature of the sample $La_{0.55}Ca_{0.45}MnO_3$, indicating a decrease in the shortest phonon wavelength. This is brought about by the decreasing of the unit-cell volume of the sample with $x=0.45$, since the shortest wavelength phonons that propagate in the crystal depend on the

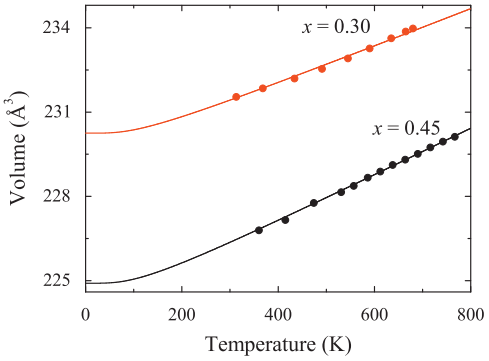

Fig. 8. Volume of the unit cell as a function of the temperature for the sample with $x=0.30$ and 0.45. Solid lines represent the fit using anharmonic theory.

Table 2
Values of the parameters obtained from the volume fitting using the anharmonic theory.

Sample	$V(T=0)$ (Å^3)	Θ_D	$9\gamma Nk_B/B$ (Å^3/K)
$x=0.30$	230.25	405.5	0.0202
$x=0.45$	224.91	410.5	0.0252

interatomic distances. Besides the variation of the Debye temperature, it is observed that the ratio γ/B is 25% larger for the sample with $x=0.45$. This may be caused by a decrease of the B ($B_{0.45}<B_{0.30}$). However, evaluation of the bulk modulus taking into account the change in the volume and specific heat at constant pression indicates that if B had influenced on γ/B, it would have been in an opposite way, namely, $B_{0.45}>B_{0.30}$ [23]. This analysis reveals that the increasing in γ/B in the sample with $x=0.45$ has a significantly contribution from an increasing of the Grüneisen parameter $[\mathrm{d}(\ln \nu)/\mathrm{d}(\ln V)]=-\gamma$. It means an increase in the phonon frequency mode with respect to the volume.

In order to check the evolution of the phonon frequency with the calcium concentration, we have measured Raman spectra at room temperature for all samples. The spectra for the samples with $x=0.20$ and 0.40 are shown in Fig. 9 which is in agreement with that found for $La_{0.70}Ca_{0.30}MnO_3$ [27]. The spectra consist of a rotational ν_1 mode and two JT activated distortions, bending ν_2 and stretching ν_3 vibration modes associated to the Mn–O–Mn octahedra [27,28]. In order to find the frequency value for each peak, a deconvolution process was done for all spectra. The deconvolution spectra for the samples with $x=0.20$ and 0.40, which are representative samples, are shown in the Fig. 9. The rotational ν_1 frequency is 229 cm^{-1} for $x=0.20$ and decreases slightly as the charge carriers are introduced

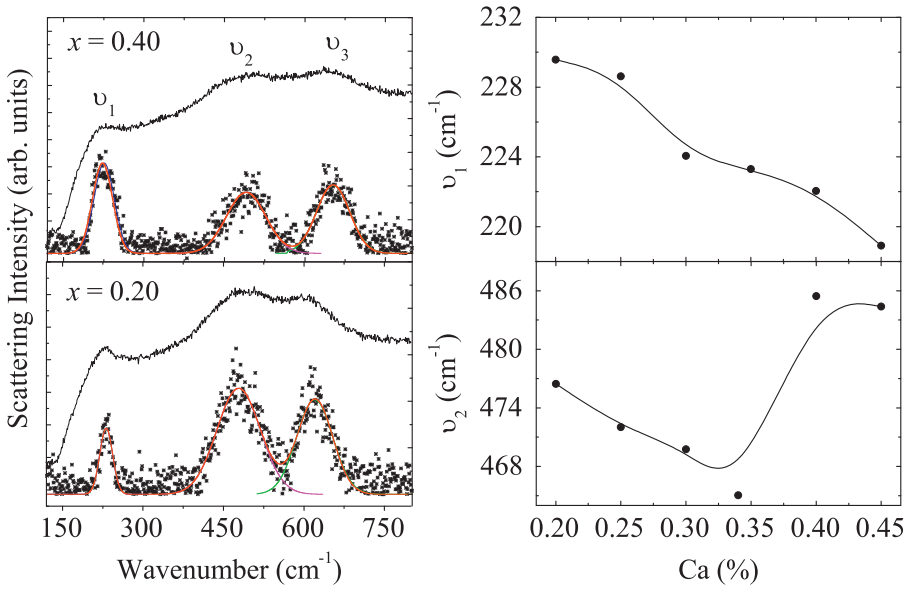

Fig. 9. (right panel) The raman spectra for the samples with $x=0.20$ and 0.40 along with the deconvoluted curves. (left panel) Rotational v_1 and bending v_2 modes as a function of Ca concentration.

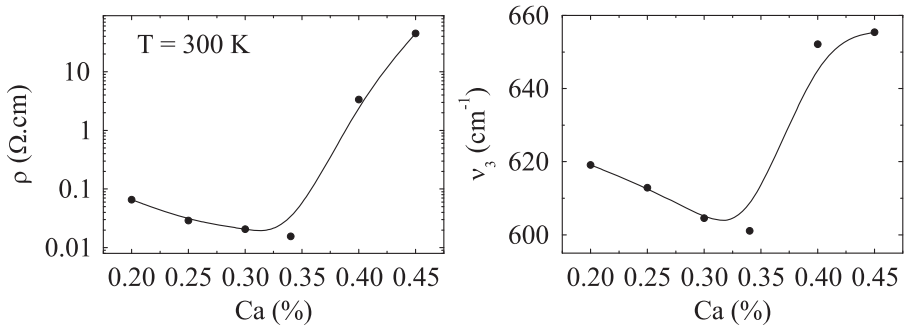

Fig. 10. The electrical resistivity (right panel) and stretching JT activated distortion mode (left panel) measured at $T=300$ K as a function of Ca doping.

assuming 218 cm^{-1} for $x=0.45$ (see Fig. 9). This evolution is different for the bending v_2 and stretching v_3 vibration modes, as shown in Figs. 9 and 10. The frequency decreases slightly for the samples up to $x=0.34$ and increases abruptly for the sample with $x=0.40$ and 0.45. This result is most pronounced for the stretching JT activated mode v_3. The electrical resistivity value obtained also at room temperature is shown in Fig. 10 in logarithm scale. Interestedly, the resistivity value also increases abruptly for the sample with $x=0.40$ as discussed above. In the small polaron model, the probability that an electron jump to a neighboring site depends on the lattice frequency [7]. The higher value of $[d(\ln v)/d(\ln V)]$ found in the sample $La_{0.55}Ca_{0.45}MnO_3$ seems to have significantly influence for which the small polaron hopping mechanism breaks down in explaining the electronic transport mechanism. In the non-adiabatic regime of small polaron model, which is defined when the relevant lattice frequency is much larger than the hopping frequency, the probability of electron hopping to neighboring sites is considered small [8]. A high value of $[d(\ln v)/d(\ln V)]$ further reduces this probability, resulting in an alteration of the electrical transport mechanism and in an abrupt increase of electrical resistivity.

4. Conclusions

In summary, we have conducted Raman spectroscopy and high-resolution X-ray diffraction, magnetization, and electrical resistivity in the high-temperature PMI state of the series $La_{1-x}Ca_xMnO_3$, with $x=0.20$, 0.25, 0.30, 0.34, 0.40 and 0.45. All samples show a structural transition close to T_{R-O}. The abrupt decreasing in the electrical resistivity observed close to the T_{R-O} due to the structural phase transition is more likely to be associated with a decreasing in the polaron activation energy (E_p) for the samples with low charge carriers. On the other hand, the data suggest a change from nonadiabatic to adiabatic regime in the samples with $x=0.30$ and 0.34 as the system goes to rhombohedral phase. The small polaron hopping mechanism is obeyed in the low doping ($0.20<x<0.34$), and breaks down for the high doping ($0.40<x<0.45$) samples where the electrical resistivity deviates from such a model. It is suggested that the more delocalized character of charge carriers observed in the samples with $x=0.20$, 0.25, 0.30 and 0.34, increases the electronic contribution to the internal energy, revealed by the temperature dependence of the thermal expansion coefficient. The deviation from small polaron hopping mechanism is consistent with an increase in the Grüneisen parameter, which is proportional to the frequency variation with respect to the volume, dv/dV. The magnetic results indicate no significantly evidence of direct correlation between the breakdown of transport mechanism and the increase of the effective magnetic moment. The change in both small polaron hopping mechanism and the electrical resistivity value is suggested to be related to the abrupt change in the bending and stretching modes as charge carriers are introduced into the system. We believe that the electronic conductivity in strong coupling spin–charge–lattice systems may be more

complex than the picture embedded in Eq. (1). However, so far, an envisaged analytical expression for the transport mechanism involving this coupling is not available. We hope the discussion presented here will attract attention to this very interesting open problem.

Acknowledgments

We are indebt with R.F. Jardim for providing conditions for the sample preparation and J.J. Neumeier for the magnetic measurements and fruitfully discussions. Raman spectroscopy measurements were carried out at Laboratório de Espectroscopia Molecular from IQ-USP, in collaboration with Dr. Romulo Augusto Ando, to whom authors are very grateful. This material is based upon work supported by the Brazilian Agencies CNPq Grant nos. 471863/2008-4, 309811/2009-0 and 307436/2008-0 and Fapesp under Grant nos. 2010/18364-0 and 2009/18618-5.

References

[1] E. Dagotto, T. Hotta, A. Moreo, Physics Reports 344 (2001) 1.
[2] E.P.-G. DeGennes, Physical Review 118 (1960) 141;
J.B. Good-enough, Physical Review 171 (1968) 466.
[3] E.O. Wollan, W.C. Koehler, Physical Review 100 (1995) 545.
[4] C. Zener, Physical Review 82 (1951) 403.
[5] P. Schiffer, A.P. Ramirez, W. Bao, S.-W. Cheong, Physical Review Letters 75 (1995) 3336.
[6] A.J. Millis, P.B. Littlewood, B.I. Shraiman, Physical Review Letters 74 (1995) 5144.
[7] R. Raffaelle, H.U. Anderson, D.M. Sparlin, P.E. Parris, Physical Review B 43 (1991) 7991.
[8] M. Jaime, H.T. Hardner, M.B. Salamon, M. Rubinstein, P. Dorsey, D. Emin, Physical Review Letters 78 (1997) 951;
M. Jaime, M.B. Salamon, M. Rubinstein, R.E. Treece, J.S. Horwitz, D.B. Chrisey, Physical Review B 54 (1996) 11914.
[9] J.H. Zhao, H.P. Kunkel, X.Z. Zhou, G. Williams, Journal of Physics: Condensed Matter 13 (2001) 5785;
A. Banerjee, S. Pal, E. Rozenberg, B.K. Chaudhuri, Journal of Physics: Condensed Matter 13 (2001) 9489.
[10] J.L. Cohn, C. Chiorescu, J.J. Neumeier, Physical Review B 72 (2005) 024422;
R. Ang, W.J. Lu, R.L. Zhang, B.C. Zhao, X.B. Zhu, W.H. Song, Y.P. Sun, Physical Review B 72 (2005) 184417;
A. Karmakar, S. Majumdar, S. Giri, Physical Review B 79 (2009) 094406.
[11] B. Munirathinam, M. Krishnaiah, S. Arumugam, M. Manivel Raja, Journal of Physics and Chemistry of Solids 71 (2010) 1763.
[12] S.K. Srivastava, S. Ravi, Journal of Superconductivity and Novel Magnetism 22 (2009) 651.
[13] R.R. Zhang, G.L. Kuang, X. Luo, Y.P. Sun, Journal of Alloys and Compounds 484 (2009) 36.
[14] Y. Kalyana Lakshmi, G. Venkataiah, M. Vithal, P. Venugopal Reddy, Physica B 403 (2008) 3059.
[15] F.F. Ferreira, E. Granado, W. Carvalho Jr., S.W. Kycia, D. Bruno, R. Droppa Jr., Journal of Synchrotron Radiation 413 (2006) 46.
[16] V. Kiryukhin, New Journal of Physics 6 (2004) 155.
[17] N.E. Hussey, K. Takenaka, H. Takagi, Philos. Mag. 84 (2004) 2847.
[18] N.F. Mott, E.A. Davies, Electron Processes in Non-crystalline Materials, Clarendon, Oxford, 1979.
[19] J.A. Souza, H. Terashita, E. Granado, R.F. Jardim, N.F. Oliveira Jr., R. Muccillo, Physical Review B 78 (2008) 054411.
[20] J.A. Souza, R.F. Jardim, Physical Review B 71 (2005) 054404.
[21] J.A. Souza, J.J. Neumeier, R.K. Bollinger, B. McGuire, C.A.M. dos Santos, H. Terashita, Physical Review B 76 (2007) 024407.
[22] S. Blundell, Magnetism in Condensed Matter, Oxford University Press, New York, 1971.
[23] L.A. Girifalco, Statical Mechanics of Solids, Oxford University Press, New York, 2000.
[24] P.G. Radaelli, M. Marezio, H.Y. Hwang, S.W. Cheong, Journal of Solid State Chemistry 122 (1996) 444.
[25] G. Wu, J.J. Neumeier, C.D. Ling, D.N. Argyriou, Physical Review B 65 (2002) 174113.
[26] T. Kiyama, K. Yoshimura, K. Kosuge, Y. Ikeda, Y. Bando, Physical Review B 54 (1996) R756.
[27] M.N. Iliev, M.V. Abrashev, Journal of Raman Spectroscopy 32 (2001) 805.
[28] E. Granado, J.A. Sanjurjo, C. Rettori, J.J. Neumeier, S.B. Oseroff, Physical Review B 62 (2000) 11304.